Photoconductive properties of PVK-based photorefractive polymer composites doped with fluorinated styrene chromophores

Eric Hendrickx, Yadong Zhang, Kyle B. Ferrio, Jon A. Herlocker, Jeff Anderson, Neal R. Armstrong, Eugene A. Mash, André P. Persoons, Nasser Peyghambarian and Bernard Kippelen

Optical Sciences Center, The University of Arizona, Tucson, AZ 85721, USA

We have synthesized nine anisotropic chromophores, with different degrees of fluorination, and studied the effect of the chromophore's ionization potential on charge-transfer complexation, photoconductivity, and response time in photorefractive polymer mixtures based on poly(vinylcarbazole). (2,4,7-Trinitrofluoren-9-ylidene)malononitrile (TNFDM) or C_{60} provided the sensitization. We have found evidence of strong complexation between TNFDM and the chromophore. At high electric fields, the photoconductivity decays during illumination and reaches a limiting value that correlates with the chromophore's ionization potential. A buildup of C_{60}^- radical anions is observed simultaneously. The strong decline in photoconductivity correlates with an increase in the photorefractive grating buildup time.

Introduction

Inorganic crystals, such as $LiNbO_3$ and $BaTiO_3$, were the first materials in which the photorefractive effect was demonstrated.[1] A theory, developed by Kukhtarev, describes this effect as the generation of a phase-shifted index modulation.[2] An internal space-charge field is established through the generation, diffusion, drift and trapping of photogenerated charge-carriers. Because of the reversibility of the photorefractive effect, photorefractive inorganic crystals are used in real-time holography for a variety of applications, such as optical correlation.

The photorefractive effect in polymers was discovered in 1991.[3] Since photorefractive polymers provide a low-cost alternative to the traditional photorefractive inorganic crystals, their properties and characterization are actively being investigated.[4] A photorefractive polymer is typically composed of a photoconductive polymer, a highly polar, anisotropic chromophore, and a sensitizer to provide absorption at the working wavelength. It has also been shown that, for low-T_g polymer composites, the main contribution to the index modulation amplitude does not stem from the electro-optic effect, but from the reorientation of the anisotropic chromophores.[5] An optimization of the dipole moment, polarizability anisotropy, and first hyperpolarizability of the chromophore using guidelines from the Bond Order Alternation theory has led to the development of polymers that have nearly complete internal diffraction at applied electric fields as low as 30 V μm^{-1}.[6]

Response times of 4 ms have been found, enabling applications at video rates.[7] It has also been demonstrated that this response time was not limited by the speed of chromophore reorientation. Since the buildup of a photorefractive grating requires photogeneration, charge transport, and reorientation it is likely that the buildup time correlates with the photoconductivity, which itself is a function of mobility and photogeneration efficiency. Here we focus on the photoconductive properties of photorefractive samples, and their influence on the four-wave mixing buildup time.

The materials studied in this paper are based on the photoconductor polyvinylcarbazole (PVK), plasticized with *N*-ethylcarbazole (ECZ). The dopant chromophores had a piperidino or homopiperidino donor, a dicyano or cyanomethoxycarbonyl acceptor and a styrene conjugated system. To systematically vary the ionization potential of the chromo-

phores, the styrene bridge of the dopant chromophore was substituted with one or more fluorine atoms. At the working wavelength of 633 nm, we have used two sensitizers: (2,4,7-trinitrofluoren-9-ylidene)malononitrile (TNFDM) and C_{60}.

In the first section of the paper, we report the synthesis of the different chromophores and the preparation of the photorefractive polymer samples. Then, we report on the properties of the chromophores, such as the ionization potential, and the charge-transfer complexes formed between TNFDM, carbazole, polyvinylcarbazole and the chromophores. In the third section we present the photoconductivity measurements performed on the different materials and the C_{60}^- concentration buildup during illumination under applied field. Finally, we show that grating buildup times increase significantly during illumination under applied field for chromophores with low ionization potential.

1 Synthesis and sample preparation

A Synthesis

The chromophores were prepared in a two-step synthesis shown in Scheme 1. A mixture of 4-fluorobenzaldehyde (1
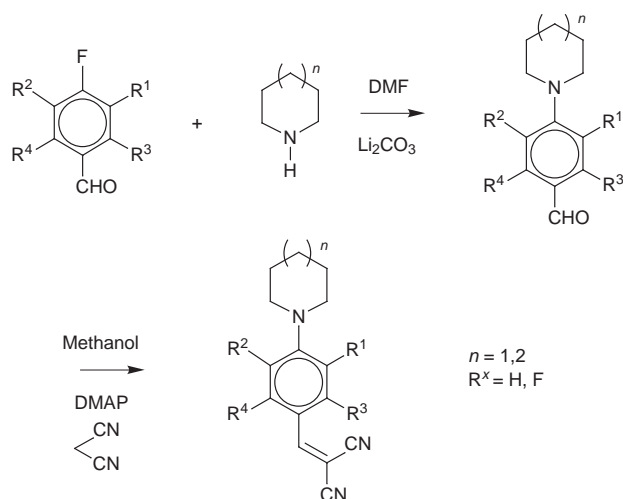
Scheme 1

equiv.), piperidine or homopiperidine (1 equiv.), lithium carbonate (5 equiv.), and DMF (20 mL) was stirred at 50 °C for 10 h. Water (200 mL) was added to the reaction mixture. The products were extracted with chloroform. After removal of chloroform, the crude products were purified by silica gel column chromatography using hexanes–ethyl acetate as eluent. 4-(Dimethylamino)pyridine (0.5 equiv.) was added to a solution of the 4-piperidinobenzaldehyde or 4-homopiperidinobenzaldehyde (1 equiv.) and malononitrile (1.5 equiv.) in methanol (15 mL). The reaction mixture was kept at room temperature and the product precipitated from the solution. The yellow product was collected by filtration and purified by recrystallization from acetone–water.

2,3,5,6-Tetrafluoro-4-piperidinobenzaldehyde. ^{1}H-NMR (CDCl₃, 200 MHz): δ (ppm) = 10.14 (s, 1 H, CHO), 3.38 (s, 4 H, 2 × CH₂), 1.72 (m, 6 H, 3 × CH₂).

2-Fluoro-4-piperidinobenzaldehyde. ^{1}H-NMR (CDCl₃, 200 MHz): δ (ppm) = 10.03 (s, 1 H, CHO), 7.67 (t, 1 H$_{arom}$), 6.64 (dd, 1 H$_{arom}$), 6.44 (dd, 1 H$_{arom}$), 3.38 (m, 4 H, 2 × CH₂), 1.66 (m, 6 H, 3 × CH₂).

2,5-Difluoro-4-piperidinobenzaldehyde. ^{1}H-NMR (CDCl₃, 200 MHz): δ (ppm) = 10.10 (d, 1 H, CHO), 7.44 (dd, 1 H$_{arom}$), 6.54 (dd, 1 H$_{arom}$), 3.27 (m, 4 H, 2 × CH₂), 1.78 (m, 6 H, 3 × CH₂).

2,5-Difluoro-4-homopiperidinobenzaldehyde. ^{1}H-NMR (CDCl₃, 200 MHz): δ (ppm) = 10.02 (d, 1 H, CHO), 7.43 (dd, 1 H$_{arom}$), 6.40 (dd, 1 H$_{arom}$), 3.53 (m, 4 H, 2 × CH₂), 1.83 (m, 4 H, 2 × CH₂), 1.65 (m, 4 H, 2 × CH₂).

2,3,5,6-Tetrafluoro-4-homopiperidinobenzaldehyde. ^{1}H-NMR (CDCl₃, 200 MHz): δ (ppm) = 10.12 (s, 1 H, CHO), 3.57 (m, 4 H, 2 × CH₂), 1.82 (m, 4 H, 2 × CH₂), 1.67 (m, 4 H, 2 × CH₂).

4-Piperidinobenzaldehyde. ^{1}H-NMR (CDCl₃, 200 MHz): δ (ppm) = 9.74 (s, 1 H, CHO), 7.70 (d, 2 H$_{arom}$, J = 8.9 Hz), 6.88 (d, 2 H$_{arom}$, J = 8.9 Hz), 3.40 (m, 4 H, 2 × CH₂), 1.67 (m, 6 H, 3 × CH₂).

4-Homopiperidinobenzaldehyde. ^{1}H-NMR (CDCl₃, 200 MHz): δ (ppm) = 9.70 (s, 1 H, CHO), 7.71 (d, 2 H$_{arom}$, J = 8.9 Hz), 6.70 (d, 2 H$_{arom}$, J = 8.9 Hz), 3.54 (m, 4 H, 2 × CH₂), 1.80 (m, 4 H, 2 × CH₂), 1.58 (m, 4 H, 2 × CH₂).

α-Cyano-4-piperidinocinnamic acid, methyl ester (1). Mp 97.8 °C. ^{1}H-NMR (CDCl₃, 200 MHz): δ (ppm) = 8.07 (s, C=C−H), 7.90 (d, 2 H$_{arom}$, J = 9.1 Hz), 6.85 (d, 2 H$_{arom}$, J = 9.1 Hz), 3.89 (s, 3 H, –OCH₃), 3.47 (m, 4 H, 2 × CH₂), 1.68 (m, 6 H, 3 × CH₂). Anal. calcd for C₁₆H₁₈N₂O₂ (270.33): C 71.09%, H 6.71%, N 10.36%; Found: C 71.12%, H 6.82%, N 10.47%.

4-Homopiperidinobenzylidenemalononitrile (2). Mp 148.3 °C. ^{1}H-NMR (CDCl₃, 200 MHz): δ (ppm) = 7.79 (d, 2 H$_{arom}$, J = 9.1 Hz), 7.43 (s, 1 H, C=C−H), 7.71 (d, 2 H$_{arom}$, J = 9.1 Hz), 3.58 (t, 4 H, 2 × CH₂), 1.82 (m, 4 H, 2 × CH₂), 1.60 (m, 4 H, 2 × CH₂). Anal. calcd for C₁₆H₁₇N₃ (251.33): C 76.46%, H 6.82%, N 16.72%; Found: C 76.29%, H 6.90%, N 16.61%.

4-Piperidinobenzylidenemalononitrile (3). Mp 128.5 °C. ^{1}H-NMR (CDCl₃, 200 MHz): δ (ppm) = 7.77 (d, 2 H$_{arom}$, J = 9.1 Hz), 7.44 (s, 1 H, C=C−H), 6.83 (d, 2 H$_{arom}$, J = 9.1 Hz), 3.49 (m, 4 H, 2 × CH₂), 1.71 (m, 6 H, 3 × CH₂). Anal. calcd for C₁₅H₁₅N₅ (237.29): C 75.93%, H 6.37%, N 17.71%; Found: C 75.74%, H 6.42%, N 17.62%.

α-Cyano-4-piperidino-2-fluorocinnamic acid, methyl ester (4). Mp 138.5 °C. ^{1}H-NMR (CDCl₃, 200 MHz): δ (ppm) = 8.40 (m, H$_{arom}$, C=C−H), 6.71 (dd, H$_{arom}$), 6.50 (dd, H$_{arom}$), 3.90 (s, 3 H, –OCH₃), 3.44 (m, 4 H, 2 × CH₂), 1.70 (m, 6 H, 3 × CH₂). Anal. calcd for C₁₆H₁₇FN₂O₂ (288.32): C 66.66%, H 5.94%, N 9.71%; Found: C 66.51%, H 5.95%, N 9.72%.

2-Fluoro-4-piperidinobenzylidenemalononitrile (5). Mp 124.2 °C. ^{1}H-NMR (CDCl₃, 200 MHz): δ (ppm) = 8.24 (t, 1 H$_{arom}$), 7.79 (s, 1 H, C=C−H), 6.67 (dd, 1 H$_{arom}$), 6.47 (dd, 1 H$_{arom}$), 3.48 (m, 4 H, 2 × CH₂), 1.71 (m, 6 H, 3 × CH₂). Anal. calcd for C₁₅H₁₄FN₃ (255.29): C 70.57%, H 5.53%, N 16.46%; Found: C 70.41%, H 5.44%, N 16.40%.

2,5-Difluoro-4-piperidinobenzylidenemalononitrile (6). Mp 139.5 °C. ^{1}H-NMR (CDCl₃, 200 MHz): δ (ppm) = 8.00 (dd, 1 H$_{arom}$), 7.82 (s, 1 H, C=C−H), 6.60 (dd, 1 H$_{arom}$), 3.39 (m, 4 H, 2 × CH₂), 1.71 (m, 6 H, 3 × CH₂). Anal. calcd for C₁₅H₁₃F₂N₃ (273.29): C 65.92%, H 4.79%, N 15.38%; Found: C 65.81%, H 4.86%, N 15.34%.

2,5-Difluoro-4-homopiperidinobenzylidenemalononitrile (7). Mp 141.5 °C. ^{1}H-NMR (CDCl₃, 200 MHz): δ (ppm) = 8.00 (dd, 1 H$_{arom}$), 7.76 (s, 1 H, C=C−H), 6.42 (dd, 1 H$_{arom}$), 3.62 (m, 4 H, 2 × CH₂), 1.84 (m, 4 H, 2 × CH₂), 1.62 (m, 4 H, 2 × CH₂). Anal. calcd for C₁₆H₁₅F₂N₃ (287.31): C 66.89%, H 5.22%, N 14.63%; Found: C 66.88%, H 5.22%, N 14.63%.

2,3,5,6-Tetrafluoro-4-homopiperidinobenzylidenemalononitrile (8). Mp 104.5 °C. ^{1}H-NMR (CDCl₃, 200 MHz): δ (ppm) = 7.63 (s, 1 H, C=C−H), 3.58 (m, 4 H, 2 × CH₂), 1.84 (m, 4 H, 2 × CH₂), 1.67 (m, 4 H, 2 × CH₂). Anal. calcd for C₁₆H₁₃F₄N₃ (323.29): C 59.45%, H 4.05%, N 13.00%; Found: C 59.21%, H 4.18%, N 12.88%.

2,3,5,6-Tetrafluoro-4-piperidinobenzylidenemalononitrile (9). Mp 112.5 °C. ^{1}H-NMR (CDCl₃, 200 MHz): δ (ppm) = 7.65 (s, 1 H, C=C−H), 3.41 (m, 4 H, 2 × CH₂), 1.70 (m, 6 H, 3 × CH₂). Anal. calcd for C₁₅H₁₁F₄N₃ (309.27): C 58.26%, H 3.59%, N 13.59%; Found: C 58.36%, H 3.52%, N 13.53%.
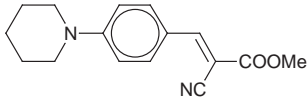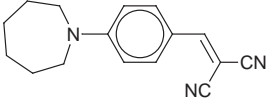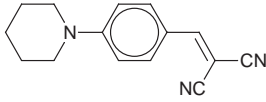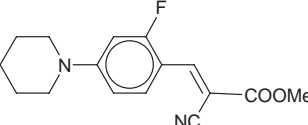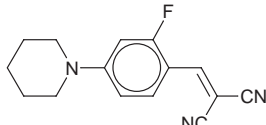
B Sample preparation

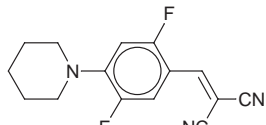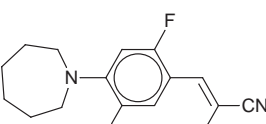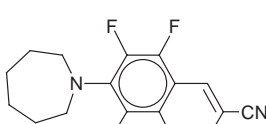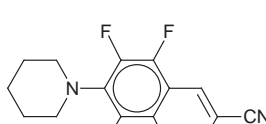Photorefractive samples had a composition of PVK : ECZ : chromophore 2 : 1 : 1 wt. ratio. TNFDM and C₆₀ were used at concentrations of 0.50 mg per 200 mg mixture and 2 mg per 200 mg mixture, respectively. The PVK–ECZ–TNFDM or C₆₀ reference samples without chromophore had a PVK : ECZ wt. ratio of 3 : 2, but identical TNFDM and C₆₀ concentrations to their photorefractive counterparts.

For the sample preparation, PVK, ECZ, chromophore and TNFDM were dissolved in anhydrous CH₂Cl₂. C₆₀ was dissolved in toluene and added to the CH₂Cl₂ solution. After filtering through an Acrodisc® filter with 0.2 μm PTFE membrane, the solvent was evaporated on a rotary evaporator. The material was dried at 65 °C and 5 cm Hg for 2–6 h to remove the residual solvent. The dried material was homogenized mechanically at 150 °C. Small pieces of the homogenized material were then sandwiched between ITO-coated glass slides at 150 °C. 105 μm glass beads were used as spacers to ensure a uniform sample thickness. The sample was then quench-cooled and sealed with epoxy glue.

The glass transition temperatures T_g of the TNFDM-based materials were measured using the reversible heat flow component in a Thermal Instruments 2920 m-DSC at an underlying heating rate of 5 °C min^{-1} and a modulation of ± 0.796 °C every 60 s. T_g values are reported in Table 1. Linear absorption spectra of the different samples were measured with a Cary 5G spectrophotometer. In the sample, the polymer is sandwiched between two parallel ITO electrodes and due to multiple reflections at these interfaces, interference fringes are

Table 1 Glass transition temperatures and extinction coefficients at 633 nm of the prepared PVK–ECZ–chromophore mixtures. Mixtures **T1**–**T9** and **C1**–**C9** had a composition of PVK–ECZ–chromophore 2:1:1 wt. ratio, **T10** and **C10** had composition PVK–ECZ 3:2 wt. ratio. TNFDM was present in 0.25 wt.%, C_{60} 1 wt.%

Chromophore structure	Chromophore number	TNFDM sample number	T_g/°C	α_{633}/cm^{-1}	C_{60} sample number	T_g/°C	α_{633}/cm^{-1}
piperidine–phenyl–CH=C(CN)COOMe	1	T1	35	29	C1	36	48
azepane–phenyl–CH=C(CN)CN	2	T2	33	32			
piperidine–phenyl–CH=C(CN)CN	3	T3	30	33	C3	34	43
piperidine–(F)phenyl–CH=C(CN)COOMe	4	T4	35	28	C4	35	40
piperidine–(F)phenyl–CH=C(CN)CN	5	T5	33	31	C5	35	35
piperidine–(F,F)phenyl–CH=C(CN)CN	6	T6	40	30	C6	37	35
azepane–(F,F)phenyl–CH=C(CN)CN	7	T7	36	29	C7	35	36
azepane–(F,F,F,F)phenyl–CH=C(CN)CN	8	T8	40	27	C8	45	34
piperidine–(F,F,F,F)phenyl–CH=C(CN)CN	9	T9	40	25	C9	38	31
None	None	T10	55	30	C10	60	37

observed in the near IR. From the spacing of these fringes, $\Delta\lambda$, the sample thickness d was calculated from eqn. (1).

$$d = \frac{\lambda^2}{2n\Delta\lambda} \qquad (1)$$

The refractive index at 1300 nm of the polymers (≈ 1.66) was measured using a Metricon 2010 prism coupler in the substrate mode. The extinction coefficient at 633 nm, α, was calculated after correcting for the sample thickness and reflection losses and is shown in Table 1.

2 Charge-transfer complexation and ionization potential

The relative position of the ionization potential of the synthesized chromophores was estimated from cyclic voltammetry. Voltammograms were recorded of 10^{-3} M solutions of chromophores in acetonitrile dried over activated alumina. Tetrabutylammonium hexafluorophosphate was used as the supporting electrolyte, the scan rate was 500 mV s^{-1} and the curves were referenced to the normal hydrogen electrode

Table 2 Positions of the anodic oxidation ($E_{p,a}$) and cathodic reduction ($E_{p,c}$) current peaks observed in the cyclic voltammograms, referenced *vs.* the NHE

Chromophore	$E_{p,a}$/mV	$E_{p,c}$/mV
1	1390	−1220
2	1500	−1230
3	1510	−1060
4	1540	−1160
5	1630	−1090
6	1710	−990
7	1730	−860
8	1890	−780
9	1910	−790

Table 3 Stability constants and molar absorptivities of the charge-transfer complexes between PVK, ECZ, chromophores **1–5**, and TNFDM

Chromophore/TNFDM	K/M^{-1}	Molar absorptivity 633 nm/M^{-1} cm^{-1}
PVK (CHCl$_3$)	8.4	490
ECZ (CHCl$_3$)	21	1400
ECZ (acetone)	16	790
1 (acetone)	3.8	880
2 (acetone)	4.2	510
3 (acetone)	4.0	510
4 (acetone)	5.9	440
5 (acetone)	5.6	250

(NHE) using ferrocene ($E^0 = 0.690$ *vs.* NHE). The results are summarized in Table 2. As can be seen from Table 2, the anodic oxidation and cathodic reduction waves shift to higher potentials upon fluorination, and the chromophores span a range of 400 mV in redox potential. Under our experimental conditions, the voltammograms for the reduction process indicated that the reduction product was not stable. Voltammograms for the oxidation process indicated that the oxidation product was stable, except for the tetrafluorinated dyes.

In most photorefractive polymers, a small amount of sensitizer is added to provide absorption at the operating wavelength. A fraction of the absorbed photons must be converted into free charges that can migrate and form a space-charge field.

One possible method of sensitizing a material is to add a small amount of a conjugated molecule substituted with electron deficient groups, such as 2,4,7-trinitrofluorenone or TNFDM. These molecules can form a charge-transfer complex with the electron-rich carbazole groups. The absorption associated with this complexation is, in general, red-shifted compared to that of the individual molecules. Since upon excitation of a charge-transfer complex an electron is transferred from the electron-rich ligand to the electron-poor ligand, charge separation and generation are initiated. Ideally, this complexation only occurs between the sensitizer and the hole transport agent. However, we have found evidence of a complexation between the anisotropic chromophore and TNFDM.

The stability constant is defined as $K = [A–D]/[A][D]$, where [A–D], [A] and [D] are the CT complex, acceptor and donor concentrations, respectively. It is a measure of the stability of the charge-transfer complex and can be determined spectro-photometrically by measuring the optical densities of a series of solutions. If the analytical donor concentration [D]$_0$ is much larger than the analytical acceptor concentration [A]$_0$, and both analytical concentrations are sufficiently small, the Benesi–Hildebrand equation can be used to calculate K and the molar absorptivity ε of the complex [eqn. (2)][8]

$$\frac{[A]_0}{A} = \frac{1}{K\varepsilon[D]_0} + \frac{1}{\varepsilon} \qquad (2)$$

A is the optical density due to the absorption of the charge-transfer complex only. If these conditions cannot be met, iterative technique can be used to solve eqn. (3).

$$\frac{[A]_0}{A} = \frac{1}{K\varepsilon[D]_0} + \frac{1}{\varepsilon} + \frac{[A]_0}{[D]_0\varepsilon} - \frac{[AD]}{\varepsilon[D]_0} \qquad (3)$$

We have determined the charge-transfer stability constants and molar absorptivities of the complexes formed between TNFDM and ECZ, PVK and some of the chromophores used. The TNFDM concentration was constant for a given donor, and the optical densities of five solutions with different donor concentrations were measured. The TNFDM and donor concentrations ranged from 0.07–0.005 M and 0.04–0.006 M,

respectively. For TNFDM–ECZ, the complexation was strong and the stability constant was calculated with the Benesi–Hildebrand eqn. (2). For the other complexes, the stability constant was calculated iteratively using eqn. (3) and the Minerr function of Mathcad 5.0. The results are summarized in Table 3.

The complexation is strongest between TNFDM and ECZ. The reduction in affinity between TNFDM and the carbazole unit in PVK can be attributed to the steric hindrance in the polymer coil. A similar reduction in affinity, related to steric hindrance, has been observed for alkylated benzenes.[8] A small, but significant equilibrium constant is found for the unfluorinated and monofluorinated chromophores. Even though the amino donor group is conjugated with a strong electron-withdrawing group, it still is able to participate in complexation. The increase in equilibrium constant upon fluorination is possibly related to stabilization of the complex by increased dipole–dipole interactions. Note that all the TNFDM–chromophore complexes in Table 3 are absorbing at 633 nm, and thus prevent a selective excitation of the TNFDM–carbazole complex in the photorefractive polymer mixture.

We have found spectroscopic evidence of complexation with TNFDM for all the chromophores used. The energy of the absorption band of the charge-transfer complex $h\nu$ correlates with the ionization potential of the donor according to eqn. (4), where

$$h\nu = aI_p + b \qquad (4)$$

a and b are constant for a given acceptor. The ionization potential of the chromophore can be estimated from the redox potential E^0 as $I_p(eV) = E^0(V) + 4.5$.[9] As can be seen from Table 4, upon fluorination the ionization potential of the chromophore increases, and the absorption band of the charge-transfer complex is shifted to smaller wavelengths. C$_{60}$ has been shown to strongly increase the photoconductivity of PVK, and decreased the grating buildup time when used as a sensitizer for photorefractive polymer films.[10] Recently, it was shown that C$_{60}$ forms a weak charge-transfer complex with

Table 4 Absorption maxima of the charge-transfer complexes formed between the chromophores listed and TNFDM, and ionization potential as measured from cyclic voltammetry. The I_p of ECZ is based on the redox potential from reference 15

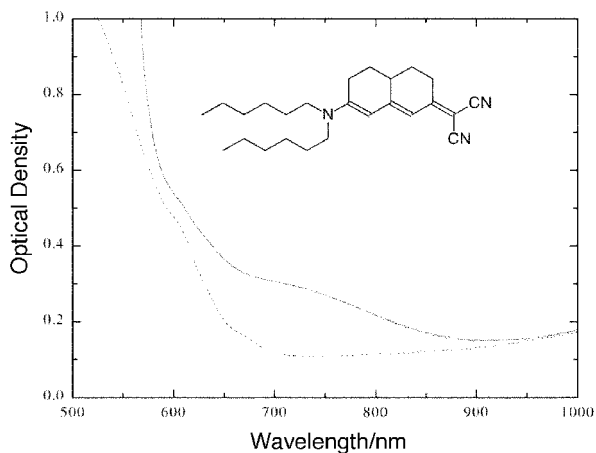| Chromophore/TNFDM	λ_{max} complex/nm	I_p/eV
1	660	5.82
2	651	5.91
3	629	5.90
4	615	5.95
5	609	6.02
ECZ	607	≈5.9
6	500	6.11
7	539	6.13
8	<550	≈6.3
9	<550	≈6.3

Fig. 1 Transmission spectrum of a PVK–ECZ–DHADC-MPN–C_{60} (100:50:50:2, solid line) and PVK–ECZ–C_{60} (120:80:2, dashed line) film between ITO-coated glass slides. The offset is due to reflections at the air/glass/ITO/polymer interfaces. The inset shows the structure of DHADC-MPN.

ECZ. An equilibrium constant of 1.5 M^{-1} was reported in methylcyclohexane, and the onset of the absorption due to complexation occurred around 600 nm.[11] Due to the low solubilities of the polar chromophores in solvents compatible with C_{60} and the small equilibrium constants, we did not find spectroscopic evidence of charge-transfer interaction between the chromophores and C_{60} in solution.

Evidence of a complexation occurring between C_{60} and a chromophore in a photorefractive polymer was found for the chromophore 2-N,N-dihexylamino-7-dicyanomethylidene-3,4,5,6,10-pentahydronaphthalene (DHADC-MPN). The I_p of DHADC-MPN calculated from cyclic voltammograms is approximately 5.4 eV, which red-shifts the absorption of the complex formed with C_{60} compared to that of the C_{60}–ECZ complex. The optical density of PVK–ECZ-based samples containing C_{60} and DHADC-MPN in Fig. 1 shows an absorption feature from 700–900 nm that is not observed in PVK–ECZ-based samples with DHADC-MPN only and can be attributed to complexation between C_{60} and DHADC-MPN.

As can be seen from Table 1, the extinction coefficients of the photorefractive polymers vary slightly from material to material. In the TNFDM-based materials, chromophore and carbazole complete for the complexation with TNFDM. For the perfluorinated materials, the replacement of a TNFDM–carbazole complex by a TNFDM–chromophore complex results in a decrease of the extinction coefficient at 633 nm, 27 and 25 cm^{-1} in **T8** and **T9**, respectively, mixtures vs. 30 cm^{-1} in **T10**.

For the C_{60} based materials, the mixtures with unfluorinated chromophores, **C1** and **C3** show the largest extinction coefficients, 48 and 43 cm^{-1}. Note that the absorption of the complexation between the nonfluorinated chromophores and TNFDM is red-shifted compared to that of ECZ–TNFDM. A similar red shift of the chromophore–C_{60} complex absorption would increase its molar absorptivity at 633 nm and can explain the increased extinction coefficient at that wavelength.

3 Photoconductivity measurements

Photogeneration and redistribution of charges through diffusion and drift are both necessary requirements for a photorefractive material. The production of free carriers is described by the photogeneration efficiency ϕ, or the number of carriers produced divided by the number of absorbed photons. The redistribution of charges is characterized by the charge mobility, μ. The photoconductivity σ is a function of

both mobility and quantum efficiency. We have calculated the photoconductivity of **T1–T10** and **C1–C10** from the amplitude of the photovoltage V_{ph} obtained by illuminating a biased standard photorefractive sample with a 100 ms pulse of a He–Ne beam of intensity 6.8 W cm^{-2} or 0.68 W cm^{-2}.[12] The photoconductivity was derived from the photocurrent i_{ph} according to eqn. (5),

$$i_{ph} = \frac{V_{ph}}{R} = \sigma(E)ES \qquad (5)$$

where R is the resistance of the resistor, in series with the sample, across which the photovoltage is measured, E is the applied electric field, and S is the illustrated area.

In this geometry, the amplitude and evolution of the photocurrent were found to vary strongly with illumination time at applied fields of 80 V μm^{-1}. Typical results, obtained for sample **C3**, are shown in Fig. 2. For a fresh sample, the photocurrent reaches steady-state only after several tens of milliseconds, and the decay of the photocurrent requires several ms. After continuously illuminating the sample for 2 h at an applied field of 80 V μm^{-1} (633 nm with 0.68 mW cm^{-2}), both photocurrent buildup and decay are faster (a few ms in a typical transient), and the amplitude has been reduced by an order of magnitude. The decay of the photocurrent amplitude with illumination time is shown in the inset of Fig. 2. The slow approach to steady-state during the first exposures indicates that a large number of charge-carriers are being trapped in the material. After long exposure, the approach to steady-state is faster, suggesting a filling of the trapping levels has occurred. These filled traps may then cause a decrease in the photocurrent amplitude because they screen the applied field.

Recently, Grunnet-Jepsen et al. reported the buildup of a steady-state C_{60}^- concentration in photorefractive polymer films under applied field and illumination.[13] The C_{60}^- number density at steady-state correlated with the value of the ionization potential of the chromophore in the photorefractive polymer film. If the ionization potential of the chromophore is smaller than that of carbazole, a carbazole radical cation can oxidize the chromophore. The chromophore radical cation then stabilizes the C_{60}^- radical anion, extending its lifetime by several minutes to hours after removal of the bias field and laser beam. The more stable the chromophore radical cation, the larger the C_{60}^- concentration that is accumulated. For the three chromophores in reference 13, a correlation was found between the ionization potential of the chromophore and the C_{60}^- number density as measured from the optical density
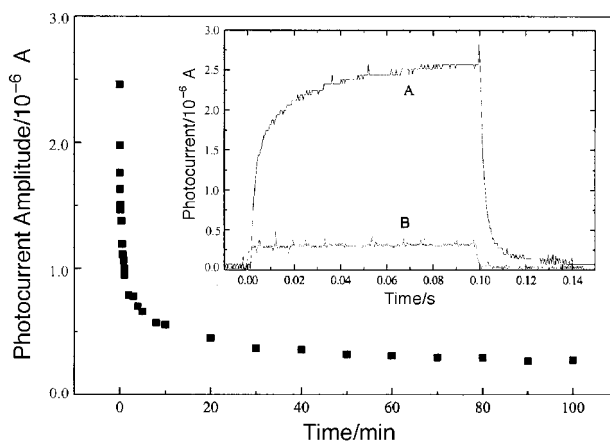

Fig. 2 Decay of the photocurrent amplitude during illumination of sample **C3** at 633 nm with 0.85 mW (area: 1.2 10^{-3} cm^2, applied field = 80 V μm^{-1}). Inset: photocurrent transient in sample **C3** measured with a 100 ms excitation pulse on spot with no previous illumination (A) and after 70 min of illumination (B).
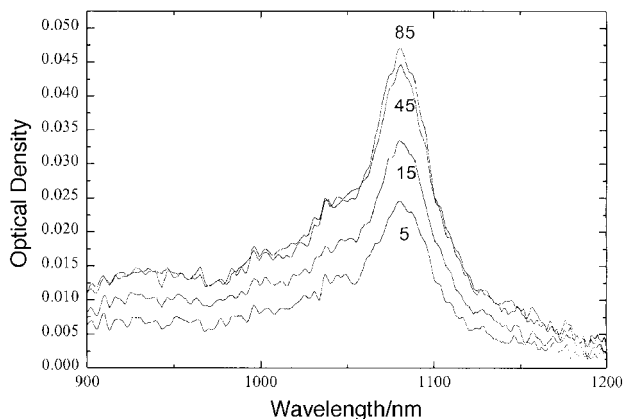
Fig. 3 Optical density change during illumination of sample **C7** at 633 nm with 30 mW cm^{-2} (illuminated area 0.2 cm^2 and power 6 mW). The spectra were recorded after exposure times of 5, 15, 45, and 85 min, respectively.

change at 1080 nm and the C$_{60}$$^-$ molar absorptivity reported in reference 14 ($\varepsilon_{peak} = 12000$ l mol^{-1} cm^{-1}).

We have found a similar correlation in eight of our C$_{60}$ based materials having chromophores with different degrees of fluorination. The samples were illuminated with an expanded beam from a He–Ne laser of intensity 30 mW cm^{-2}, and an electric field of 80 V μm^{-1} was applied. The C$_{60}$$^-$ buildup was followed optically, and a steady-state value was reached in 2 h. Fig. 3 shows the evolution of the absorption spectrum of **C7** during the measurement. The correlation between the steady-state C$_{60}$$^-$ number density and the ionization potential of the chromophore is shown in Fig. 4.

After the C$_{60}$$^-$ concentration reaches its steady-state, a correlation is found between the steady-state photoconductivity and the ionization potential of the chromophore. This dependency is shown in Fig. 5.

The photogeneration efficiency can be estimated from the steady-state photoconductivity *before* appreciable buildup of the space-charge field occurs. The photoconductivity is related to the number density of charge-carriers n_D by eqn. (6), where μ is the mobility.

$$\sigma(E) = n_D e \mu \qquad (6)$$

n_D is given by eqn. (7),

$$n_D = \phi(E) \frac{I \alpha \tau}{\hbar \omega} \qquad (7)$$

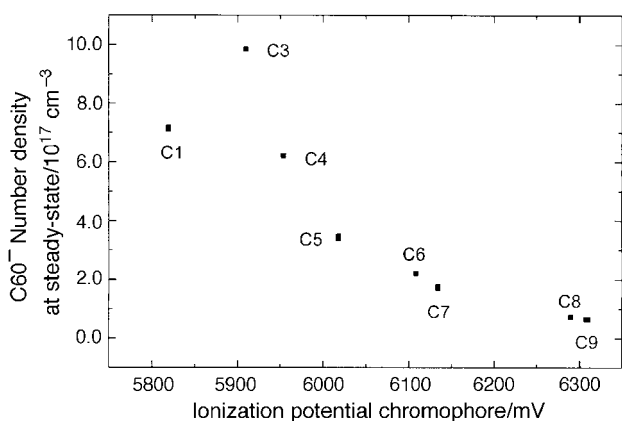where τ is the carrier lifetime. τ can be approximated by the

Fig. 4 Correlation between the steady-state C$_{60}$$^-$ number density obtained after illumination at 633 nm with 30 mW cm^{-2} (illuminated area 0.2 cm^2 and power 6 mW) at an applied electric field of 80 V μm^{-1} and the chromophore ionization potential.
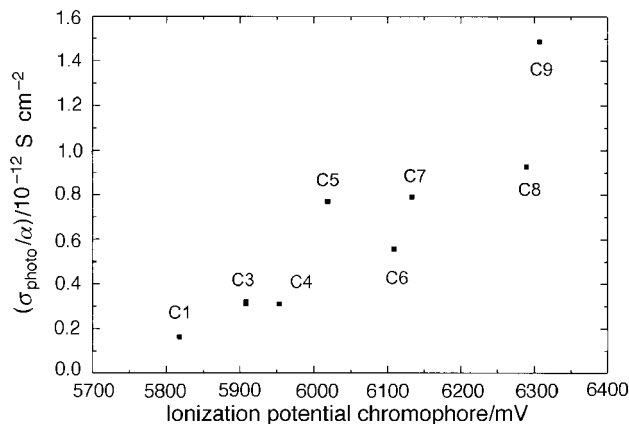
Fig. 5 Correlation between photoconductivity normalized by the extinction coefficient and the chromophore ionization potential, after the steady-state C$_{60}$$^-$ number density is obtained by illumination at 633 nm with 30 mW cm^{-2} (illuminated area 0.2 cm^2 and power 6 mW) at an applied electric field of 80 V μm^{-1}.

average transit time [eqn. (8)].

$$\tau = \frac{d}{2\mu E} \qquad (8)$$

The factor of 2 takes into account that the charge-carriers are generated uniformly throughout the weakly absorbing sample and thus travel an average distance $d/2$, where d is the sample thickness. Combining eqn. (6)–(8) gives eqn. (9) for the photogeneration efficiency.

$$\phi(E) = \frac{2\sigma(E) E \hbar \omega}{e \alpha d I} \qquad (9)$$

The quantum efficiencies for the PVK–ECZ–chromophore–TNFDM or C$_{60}$ mixtures at applied electric fields of 40 and 80 V μm^{-1} are summarized in Table 5. For the TNFDM-based materials, the addition of 25 wt.% of chromophore leads to at least a twofold reduction in ϕ at low fields and a fourfold reduction at higher fields. According to the Onsager model for the field dependence of ϕ, the increase in the dielectric constant due to the higher chromophore loading would lead to a higher value of ϕ. Possibly, this reduction in ϕ is related to the complexation occurring between the chromophore and TNFDM. Note that, for the TNFDM-sensitized polymers, increased chromophore fluorination leads to an increase in ϕ for the materials doped with chromophores with a piperidino donor, but to a reduction in ϕ for materials having a chromophore with a homopiperidino donor. Doubling the value of the applied field from 40 to 80 V μm^{-1} leads to an average increase in ϕ by a factor of 19 and 51 for the undoped TNFDM and C$_{60}$ based materials **T10** and **C10**, respectively. Doping the materials with a polar chromophore reduces this increase to 13 ± 2 and 21 ± 4 for the TNFDM and C$_{60}$ based materials, respectively. The photogeneration efficiency for the C$_{60}$ based materials is significantly higher than that of the TFNDM based materials, and is not as strongly affected by the chromophore doping.

4 Four-wave mixing experiments

We have verified the effect of the reduction of the photoconductivity on the response time of materials **C3**, **C5** and **C8**. Four-wave mixing experiments were done at 633 nm with s-polarized writing beams and a p-polarized probe beam. The angle between the bisector of the two writing beams and the sample normal was 60° and the angle between the writing beams was adjusted to provide a 3.1 μm grating spacing in the material ($\approx 20°$). The writing beams had equal optical powers of 0.45 mW, leading to a total optical power of 0.5 mW on the

Table 5 Photoconductivity of materials **T1–10** and **C1–10** measured at 633 nm and at applied fields of 40 and 80 V μm^{-1}. The optical power was 8.5 mW and the illuminated area 1.2 10^{-3} cm². Italic: photogeneration quantum efficiency ϕ calculated from eqn. (9)

TNFDM number	40 V μm^{-1} $\sigma_{photo}/nS\ cm^{-1}$ ϕ (%)	80 V μm^{-1} $\sigma_{photo}/nS\ cm^{-1}$ ϕ (%)	C_{60} number	40 V μm^{-1} $\sigma_{photo}/nS\ cm^{-1}$ ϕ (%)	80 V μm^{-1} $\sigma_{photo}/nS\ cm^{-1}$ ϕ (%)
T1	0.099 *0.0094*	0.87 *0.14*	**C1**	1.6 *0.078*	15 *1.5*
T2	0.50 *0.040*	3 *0.40*			
T3	0.089 *0.0060*	0.6 *0.088*	**C3**	2.8 *0.16*	24 *2.8*
T4	0.22 *0.0144*	1.7 *0.22*	**C4**	1.6 *0.10*	14 *1.7*
T5	0.39 *0.032*	2.3 *0.38*	**C5**	2.4 *0.15*	31 *4.2*
T6	0.27 *0.020*	2 *0.28*	**C6**	1.7 *0.11*	20 *2.8*
T7	0.35 *0.032*	2.4 *0.42*	**C7**	1.3 *0.098*	14 *1.9*
T8	0.30 *0.034*	1.8 *0.44*	**C8**	1.0 *0.098*	7.8 *1.9*
T9	0.32 *0.022*	2.3 *0.24*	**C9**	1.5 *0.11*	19 *2.4*
T10	1.3 *0.086*	11 *1.7*	**C10**	1.7 *0.090*	41 *4.6*

polymer, after correction for reflection losses. The beams were collimated to a spot size of approximately 500 µm. The optical power of the probe beam was 4 µW.

The measurements of the grating buildup time were done as follows: an electric field of 40 V μm^{-1} was applied to the sample, and the sample was illuminated with one of the two writing beams and the probe beam for 100 ms. Then, the second writing beam illuminated the sample for 1 s and the evolution of the diffracted beam was recorded. The photocurrent generated in the sample was measured simultaneously. This procedure was repeated after consecutive exposures to one of the writing beams at an applied electric field of 80 V μm^{-1}. The response time was estimated as the time required to reach half of the steady-state diffraction efficiency. The results are summarized in Fig. 6.

The response time of material **C9** remained approximately constant. For samples **C5** and **C3**, a longer exposure led to a strong increase in the four-wave mixing buildup time. Photoconductivities after ≈ 8000 s were 5 10^{-12}, 2.1 10^{-12}, 1.6 10^{-12} S cm^{-1} for **C9**, **C5**, and **C3**, respectively. While response times of the materials before exposure were similar, after long exposure, the response times correlated with the

C_{60}^- number density, obtained as described in the previous paragraph, and the photocurrent observed during the four-wave mixing experiments.

These experiments clearly demonstrate the effect of sample preconditioning on the dynamics of photorefractive grating buildup. If samples are illuminated with a high bias field applied prior to the experiment, this preconditioning can reduce the observed response time. A comparison between material response times is thus only meaningful for materials that have received identical preconditioning.

Conclusion

We have synthesized nine chromophores with different degrees of fluorination to vary the ionization potential. All the chromophores were found to form a charge-transfer complex with the sensitizer TNFDM in solution, and the absorption maximum of the complex correlates with the chromophore ionization potential. The photogeneration efficiencies of the TNFDM-based photorefractive samples were significantly smaller than these of the C_{60}-based samples.

Upon illumination of a photorefractive material sensitized with C_{60}, a fraction of the C_{60} is ionized. Simultaneously, we observed a reduction in the photoconductivity and an increase in the photorefractive grating buildup time. The steady-state C_{60}^- number density, photoconductivity, and grating buildup time correlate with the chromophore ionization potential. A chromophore with high ionization potential did not show a strong deterioration of the response time with exposure at high field, suggesting these materials have the best potential for high-speed photorefractive devices. These results suggest that there is a trade-off between high dynamic range and fast response time, however, more detailed studies in different chromophores are needed before general structure–property relationships can be established.
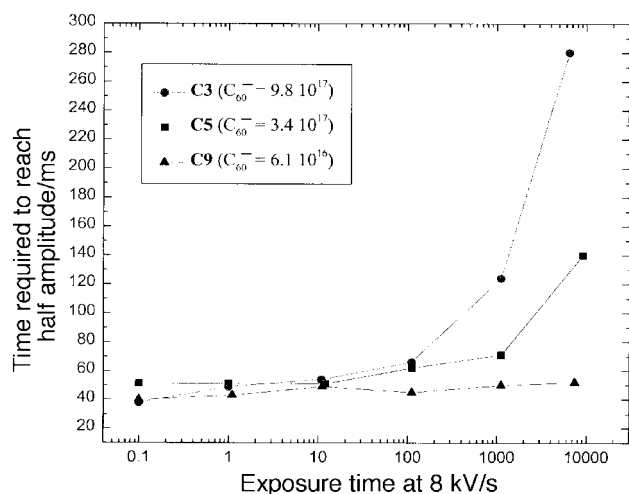

Fig. 6 Evolution of the time required to reach half the steady-state diffraction efficiency at an applied bias of 4 kV as a function of exposure to one writing beam at 8 kV.

References

1   P. Günter and J.-P. Huignard, in *Photorefractive Materials and Their Applications I&II*, Springer-Verlag, Berlin, 1988&1989.
2   N. V. Kukhtarev, V. B. Markus, S. G. Odulov, M. S. Soskin and V. L. Vinetskii, *Ferroelectrics*, 1979, **22**, 949.
3   S. Ducharme, J. C. Scott, R. J. Twieg and W. E. Moerner, *Phys. Rev. Lett.*, 1991, **66**, 1846.
4   W. E. Moerner and S. M. Silence, *Chem. Rev.*, 1994, **94**, 127.
5   W. E. Moerner, S. M. Silence, F. Hache and G. C. Bjorklund, *J. Opt. Soc. Am. B*, 1994, **11**, 320.
6   B. Kippelen, S. R. Marder, E. Hendrickx, J. L. Maldonado, G. Guillemet, B. L. Volodin, D. D. Steele, Y. Enami, Sandalphon, Y. J. Yao, J. F. Wang, H. Rockel, L. Erskine and N. Peyghambarian, *Science*, 1998, **279**, 54.
7   J. A. Herlocker, K. B. Ferrio, E. Hendrickx, B. D. Guenther, S. Mery, B. Kippelen and N. Peyghambarian, *Appl. Phys. Lett.*, 1999, **74**, 2253.
8   R. Foster, in *Organic charge-transfer complexes*, Academic Press, London and New York, 1969.
9   H. Reiss and A. Heller, *J. Phys. Chem.*, 1985, **89**, 4207.
10 S. M. Silence, C. A. Walsh, J. C. Scott and W. E. Moerner, *Appl. Phys. Lett.*, 1992, **61**, 2967.
11 Y. Wang and A. Suna, *J. Phys. Chem. B*, 1997, **101**, 5627.
12 B. Kippelen, K. Meerholz and N. Peyghambarian, in *Nonlinear Optics of Organic Molecules and Polymers*, H. S. Nalwa and S. Miyata, eds., CRC, Boca Raton, 1997.
13 A. Grunnet-Jepsen, D. Wright, B. Smith, M. S. Bratcher, M. S. DeClue, J. S. Siegel and W. E. Moerner, *Chem. Phys. Lett.*, 1998, **291**, 553.
14 M. A. Greaney and S. M. Gorun, *J. Phys. Chem.*, 1991, **95**, 7142.
15 J. F. Ambrose and R. F. Nelson, *J. Electrochem. Soc.*, 1968, **115**, 1159.

Paper 9/02745I